

# Optimal higher-lying band gaps for photonic crystals with large dielectric contrast

Ruey-Lin Chern\* and Sheng D. Chao

*Institute of Applied Mechanics, National Taiwan University, Taipei 106, Taiwan, Republic of China*

\*Corresponding author: [chern@iam.ntu.edu.tw](mailto:chern@iam.ntu.edu.tw)

**Abstract:** We investigate the characteristics of higher-lying band gaps for two-dimensional photonic crystals with large dielectric contrast. An optimal common band gap is attained on a hexagonal lattice of circular dielectric cylinders at relatively higher bands. The corresponding TM and TE modes exhibit simultaneous band edges, around which the frequency branches tend to be dispersionless. Unlike the fundamental band gap which usually appears between the dielectric and air bands, the optimal higher-lying gap in the present study occurs between two consecutive dielectric-like bands with high energy fill factors. The underlying mechanism is illustrated with the apparent change of eigenmode patterns inside the dielectric regions for both polarizations. In particular, the common gap region is bounded by two successive orders of Mie resonance frequencies on a single dielectric cylinder with the same geometry and material, where the Mie resonance modes show similar internal fields with the respective eigenmodes for the photonic crystal.

© 2008 Optical Society of America

**OCIS codes:** (160.5298) Photonic crystals; (260.5740) Resonance; (290.4020) Mie theory.

---

## References and links

1. E. Yablonovitch, "Inhibited Spontaneous Emission in Solid-State Physics and Electronics," *Phys. Rev. Lett.* **58**, 2059–2062 (1987).
2. S. John, "Strong localization of photons in certain disordered dielectric superlattices," *Phys. Rev. Lett.* **58**, 2486–2489 (1987).
3. J. D. Joannopoulos, R. D. Meade, and J. N. Winn, *Photonic Crystals: Molding the Flow of Light* (Princeton University Press, 1995).
4. A. Moroz and A. Tip, "Resonance-induced effects in photonic crystals," *J. Phys. Condens. Matter* **11**, 2503–2512 (1999).
5. E. Lidorikis, M. M. Sigalas, E. N. Economou, and C. M. Soukoulis, "Gap deformation and classical wave localization in disordered two-dimensional photonic-band-gap materials," *Phys. Rev. B* **61**, 458–13,464 (2000).
6. R. D. Meade, A. M. Rappe, K. D. Brommer, and J. D. Joannopoulos, "Nature of the photonic band gap: some insights from a field analysis," *J. Opt. Soc. Am. B* **10**, 328–332 (1993).
7. J. D. Joannopoulos, P. R. Villeneuve, and S. Fan, "Photonic crystals: putting a new twist on light," *Nature* **386**, 143–149 (1997).
8. R. D. Meade, K. D. Brommer, A. M. Rappe, and J. D. Joannopoulos, "Existence of a photonic band gap in two dimensions," *Appl. Phys. Lett.* **61**, 495–497 (1992).
9. P. R. Villeneuve and M. Piché, "Photonic band gaps in two-dimensional square and hexagonal lattices," *Phys. Rev. B* **46**, 4969–4972 (1992).
10. R. L. Chern, C. C. Chang, C. C. Chang, and R. Hwang, "Large full band gaps for photonic crystals in two dimensions computed by an inverse method with multigrid acceleration," *Phys. Rev. E* **68**, 26,704 (2003).

11. H. K. Fu, Y. F. Chen, R. L. Chern, and C. C. Chang, "Connected hexagonal photonic crystals with largest full band gap," *Opt. Express* **13**, 7854–7860 (2005).
12. R. L. Chern, C. C. Chang, C. C. Chang, and R. R. Hwang, "Two Classes of Photonic Crystals with Simultaneous Band Gaps," *Jpn. J. Appl. Phys.* **43**, 3484–3490 (2004).
13. D. Cassagne, C. Jouanin, and D. Bertho, "Hexagonal photonic-band-gap structures," *Phys. Rev. B* **53**, 7134–7142 (1996).
14. C. S. Kee, J. E. Kim, and H. Y. Park, "Absolute photonic band gap in a two-dimensional square lattice of square dielectric rods in air," *Phys. Rev. E* **56**, 6291–6293 (1997).
15. L. Shen, S. He, and S. Xiao, "Large absolute band gaps in two-dimensional photonic crystals formed by large dielectric pixels," *Phys. Rev. B* **66**, 165,315 (2002).
16. M. M. Sigalas, C. M. Soukoulis, C. T. Chan, and D. Turner, "Localization of electromagnetic waves in two-dimensional disordered systems," *Phys. Rev. B* **53**, 8340–8348 (1996).
17. M. Straub, M. Ventura, and M. Gu, "Multiple Higher-Order Stop Gaps in Infrared Polymer Photonic Crystals," *Phys. Rev. Lett.* **91**, 43,901 (2003).
18. L. Shen, Z. Ye, and S. He, "Design of two-dimensional photonic crystals with large absolute band gaps using a genetic algorithm," *Phys. Rev. B* **68**, 35,109 (2003).
19. J. Y. Ye, V. Mizeikis, Y. Xu, S. Matsuo, and H. Misawa, "Fabrication and optical characteristics of silicon-based two-dimensional photonic crystals with honeycomb lattice," *Opt. Commun.* **211**, 205–213 (2002).
20. J. Y. Ye, S. Matsuo, V. Mizeikis, and H. Misawa, "Silicon-based honeycomb photonic crystal structures with complete photonic band gap at 1.5  $\mu\text{m}$  wavelength," *J. Appl. Phys.* **96**, 6934 (2004).
21. R. L. Chern, C. C. Chang, C. C. Chang, and R. R. Hwang, "Numerical Study of Three-Dimensional Photonic Crystals with Large Band Gaps," *J. Phys. Soc. Jpn.* **73**, 727–737 (2004).
22. C. C. Chang, J. Y. Chi, R. L. Chern, C. C. Chang, C. H. Lin, and C. O. Chang, "Effect of the inclusion of small metallic components in a two-dimensional dielectric photonic crystal with large full band gap," *Phys. Rev. B* **70**, 75,108 (2004).
23. K. Ohtaka and Y. Tanabe, "Photonic Band Using Vector Spherical Waves. I. Various Properties of Bloch Electric Fields and Heavy Photons," *J. Phys. Soc. Jpn.* **65**, 2265–2275 (1996).
24. M. G. Salt and W. L. Barnes, "Flat photonic bands in guided modes of textured metallic microcavities," *Phys. Rev. B* **61**(16), 11,125–11,135 (2000).
25. J. Plouin, E. Richalot, O. Picon, M. Carras, and A. de Rossi, "Photonic band structures for bi-dimensional metallic mesa gratings," *Opt. Express* **14**, 9982–9987 (2006).
26. R. L. Chern, C. C. Chang, and C. C. Chang, "Analysis of surface plasmon modes and band structures for plasmonic crystals in one and two dimensions," *Phys. Rev. E* **73**, 36,605 (2006).
27. C. F. Bohren and D. R. Huffman, *Absorption and scattering of light by small particles* (John Wiley & Sons, New York, 1983).
28. C. A. Balanis, *Advanced Engineering Electromechanics* (John Wiley & Sons, New York, 1989).
29. C. Rockstuhl, U. Peschel, and F. Lederer, "Correlation between single-cylinder properties and bandgap formation in photonic structures," *Opt. Lett.* **31**, 1741–1743 (2006).
30. D. M. Pozar, *Microwave engineering, 3rd ed.* (Wiley, New York, 2005).
31. R. C. Kell, A. C. Greenham, and G. C. E. Olds, "High-Permittivity Temperature-Stable Ceramic Dielectrics with Low Microwave Loss," *J. Am. Ceram. Soc.* **56**, 352–354 (1973).

---

## 1. Introduction

Photonic crystals have been the subject of intensive research in the past two decades [1, 2, 3]. One of the most distinguished features is the existence of photonic band gap. Formation of band gap is considered as a result of hybridization of individual Mie resonance due to single scatterers and the Bragg-like multiple scattering due to periodicity [4]. The former corresponds to a strongly localized photon state, and the latter to a nearly free photon state [5]. Nature of photonic band gap was elucidated with the variation of electrical energy inside the dielectric regions, through the use of a fill factor [6]. As two consecutive bands exhibit markedly different fill factors, the discrepancy in frequency will be large and the band gap would be significant.

Due to the vector nature of electromagnetic fields, band gaps for two-dimensional structures behave in different manners for different polarizations. The common band gap for TM and TE modes (with respect to the normal of lattice plane) is an important issue for confining the light from arbitrary orientation. A general rule of thumb was proposed to characterize the band gap features for two-dimensional crystals: TM band gaps are favoured in a lattice of isolated high dielectric region, and TE gaps are favoured in a connected lattice [7]. This rule is useful for

describing the basic features of a fundamental band gap. A compromise between an isolated and a connected lattice then leads to a common band gap for both polarizations. One typical example is the triangular lattice of air columns [8, 9]. By incorporating two geometric parameters, the band gap size can be enlarged. The connected hexagonal lattice has an optimal common band gap (over 24%) for the silicon-air structure (with the dielectric contrast 13) [10, 11]. As the optimal condition is reached, the corresponding TM and TE modes exhibit *simultaneous* band edges. Accordingly, the common gap width is not trimmed off for either polarization [10, 12].

The higher-lying band gap (which occurs at relatively higher frequency branches) shows a different characteristic. It is not necessary for the structure to be connected [13, 14, 15]. As the mid-gap frequency is higher, the minimum feature size is larger. This can be a very important issue in fabrication [7]. However, higher-lying band gaps are more difficult to appear [16] and receive much less attention in the past [17]. This may be attributed to a more complicated behavior at higher-order Bragg scattering. Although a genetic algorithm based on the selection of dielectric pixels can be utilized to obtain a large higher-lying band gap [18], the rule or mechanism for opening optimal gaps at higher bands still demands a further study.

In this article, we investigate the features of higher-lying band gaps for two-dimensional photonic crystals. The hexagonal lattice of circular cylinders, consisting of two dielectric *atoms* in one unit cell, is used to seek for a large higher-lying band gap. Experimental and numerical studies of the hexagonal structures fabricated in silicon have demonstrated the pronounced band gap effect [19, 20]. In the present study, an optimal gap ratio is attained at a large dielectric contrast. The corresponding TM and TE modes exhibit simultaneous band edges, as in the case of fundamental optimal band gap. Two features associated with the higher-lying band gaps are different from the low-order ones. First, the band gap does not appear between the dielectric and air bands; instead, it occurs between two consecutive dielectric-like bands, where the field energy is strongly concentrated in the dielectric regions. Second, the frequency branches around the band edges become dispersionless or insensitive to the change of wave vectors. The corresponding modes are represented as flattened bands within small band widths for both polarizations in the whole wave vector space. The underlying mechanism for opening large higher-lying band gaps can be understood by the apparent change of eigenmode patterns between the upper and lower band edges. This feature is closely related to Mie resonances and waveguide modes on a single cylinder with the same geometry and material. In particular, the common band gap is bounded by two successive orders of Mie resonance frequencies, and the Mie resonance modes show similar internal field patterns with the respective eigenmodes for the photonic crystal.

## 2. Basic equations

Consider a periodic lattice of dielectric cylinders whose geometry is constant along the cylinder axis. For propagation of waves parallel to the lattice plane, the time-harmonic electromagnetic modes (with time dependence  $e^{-i\omega t}$ ) are described as

$$-\nabla^2 E = \epsilon \left( \frac{\omega}{c} \right)^2 E, \quad (1)$$

$$-\nabla \cdot \left( \frac{1}{\epsilon} \nabla H \right) = \left( \frac{\omega}{c} \right)^2 H, \quad (2)$$

for transverse magnetic (TM) and transverse electric (TE) polarizations, respectively, where  $E$  and  $H$  are field components along the cylinder axis. For periodic structures with infinite extent, it is sufficient to solve the problem in one unit cell, along with the Bloch condition

$$\phi(\mathbf{r} + \mathbf{a}_i) = e^{i\mathbf{k} \cdot \mathbf{a}_i} \phi(\mathbf{r}), \quad (3)$$

applying at the unit cell boundary, where  $\phi$  is either  $E$  or  $H$  field,  $\mathbf{k}$  is the Bloch wave vector, and  $\mathbf{a}_i$  ( $i = 1, 2$ ) is the lattice translation vector. For convenience in computation, the primitive unit cell (a hexagon) is replaced by a rectangle with the same area (cf. the right of Fig. 2). Accordingly, the lattice vectors are changed to  $\mathbf{a}_1 = (a, 0)$  and  $\mathbf{a}_2 = (a/2, \sqrt{3}a/2)$ , where  $a$  is the lattice period.

The eigensystems (1) and (2) are solved by the inverse iteration method [10, 21], in which the *Hermitian* property of the differential operators is of full use. An arbitrary distribution of fields over the unit cell is given as the initial guess of the eigenfunction, and the Rayleigh quotients

$$Q_E = \frac{\int |\nabla E|^2 d\tau}{\int \epsilon |E|^2 d\tau}, \quad Q_H = \frac{\int \frac{1}{\epsilon} |\nabla H|^2 d\tau}{\int |H|^2 d\tau}, \quad (4)$$

are employed to calculate the eigenfrequencies for TM and TE modes, respectively. By repeatedly solving a matrix inversion, the solution is refined through iterations until it is converged. The Rayleigh quotients (4) are utilized not only for obtaining the solutions, but also in the analysis of band gap features for different polarizations [22]. Details of the inverse iteration method can be found in Ref. [10].

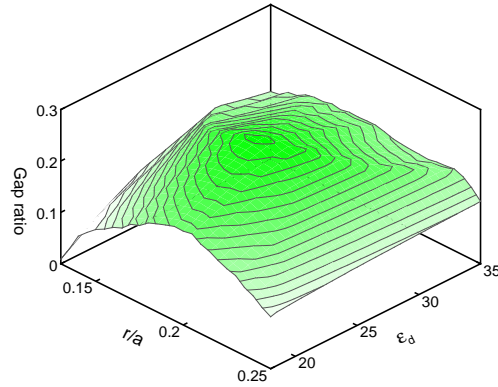


Fig. 1. Contours of the higher-lying common gap ratio for a hexagonal lattice of circular cylinders with varying the dielectric constant  $\epsilon_d$  and cylinder radius  $r/a$ .

### 3. Results and discussion

#### 3.1. Band gap features and localized modes

The hexagonal lattice of circular cylinders, where there are two dielectric *atoms* in one unit cell, is useful for studying higher-lying band gaps [7]. In order to seek for an optimal condition, two parameters have been incorporated to arrange the structures [10]. In the present study, the optimal structure is attained by increasing the dielectric contrast on one hand, and varying the cylinder radius on the other. Let the dielectric constant of the cylinder be  $\epsilon_d$ , and that of the surrounding medium be unity. Figure 1 shows the contours of higher-lying common gap ratio with respect to  $\epsilon_d$  and the cylinder radius  $r/a$ . The optimal condition is reached at  $r/a = 0.19$  and  $\epsilon_d = 26$ , and the corresponding band structure is plotted in Fig. 2. A common band gap is opened between the third and fourth bands for TE polarization, and between the sixth and seventh bands for TM polarization. The lower and upper band edges occur at  $\omega = 0.446(2\pi c/a)$  and  $0.575(2\pi c/a)$ , respectively, with a band gap width  $0.129(2\pi c/a)$  and the gap to mid-gap ratio 25.3%.

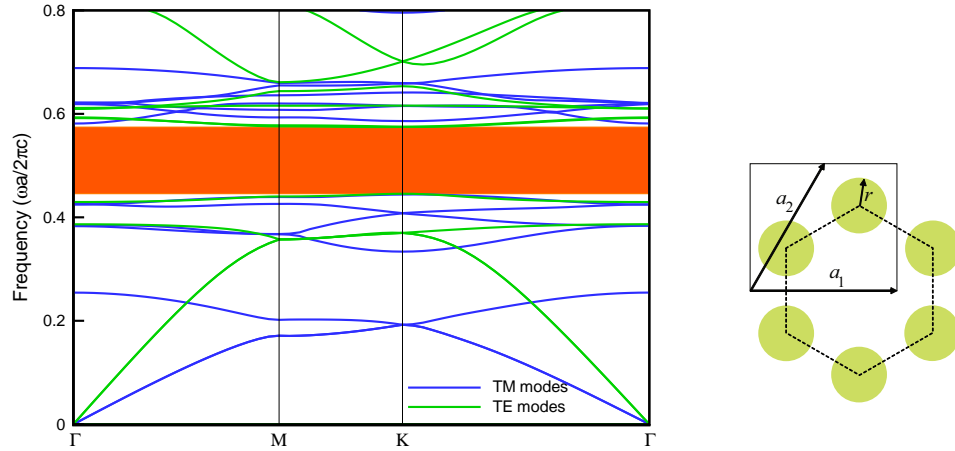


Fig. 2. Band structure for a hexagonal lattice of circular cylinders with radius  $r/a = 0.19$  and dielectric constant  $\epsilon_d = 26$ . Shaded area is the common band gap for both polarizations; the band gap width is  $0.129(2\pi c/a)$  and the gap to mid-gap ratio is 25.3%. The unit cell and geometric parameters are shown on the right.

It is noticed that the corresponding TM and TE modes exhibit *simultaneous* band edges, as has been observed in the fundamental (low-order) optimal band gap for a connected hexagonal structure [10]. The common gap width is therefore not trimmed off for either polarization. Around the band edges, the frequency branches become flattened over the whole wave vector space, which means that the resonant modes are dispersionless or insensitive to the change of Bloch wave vector. This is a typical feature of strong resonance and has been termed as the heavy photon state [23]. In the present study, the band flattening is a consequence of large dielectric contrast, as the energy has been strongly confined within the dielectric material and the frequency becomes insensitive to the change of wave vector. This phenomenon appears in other structures as well, such as the textured metallic microcavities [24], bi-dimensional metallic mesa gratings [25], and periodic arrays of plasmonic cylinders [26].

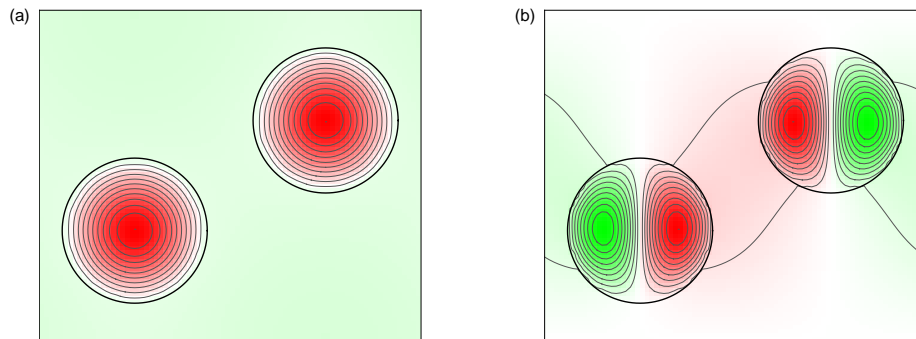


Fig. 3. Magnetic field contours of the TE eigenmodes at the point  $\Gamma$  for the photonic crystal in Fig. 2. (a) eigenmode near the lower edge with  $\omega = 0.429(2\pi c/a)$ , (b) eigenmode near the upper edge with  $\omega = 0.593(2\pi c/a)$ .

Figure 3 shows the TE eigenmode patterns near the band edges at the point  $\Gamma$ . The fields are strongly localized within the dielectric regions, where a lump of *inphase* oscillation is associated with the lower band edge [Fig. 3(a)], and a pair of *antiphase* oscillations is with the upper band edge [Fig. 3(b)]. Unlike the fundamental band gap which are likely to appear between the dielectric and air bands, the higher-lying gap in the present problem occurs between two consecutive dielectric-like bands with high energy fill factors. The fill factor  $f \equiv \int_{\epsilon=\epsilon_d} u da / \int u da$  ( $u = \epsilon\epsilon_0 E^2 + \mu_0 H^2$ ) for measuring the energy concentration within the dielectric regions [6] does not exhibit a marked difference. In Figs. 3(a) and 3(b),  $f = 0.9$  and  $0.88$ , respectively.

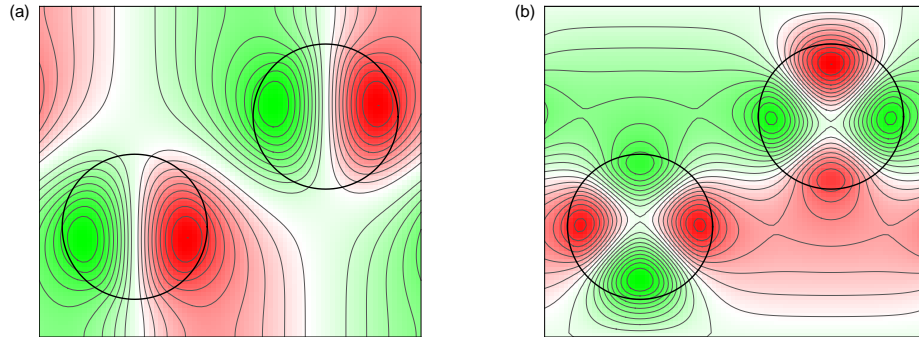


Fig. 4. Electric field contours of the TM eigenmodes at the point  $\Gamma$  for the photonic crystal in Fig. 2. (a) eigenmode near the lower edge with  $\omega = 0.425(2\pi c/a)$ , (b) eigenmode near the upper edge with  $\omega = 0.618(2\pi c/a)$ .

Similar localized field patterns of the respective eigenmodes are observed for TM polarization as well, as shown in Fig. 4. The fill factors are still large for both modes;  $f = 0.79$  and  $0.87$  for Figs. 4(a) and 4(b), respectively. However, the field localization within the dielectric regions are not so strong. This is due to the boundary condition for tangential  $E$  field, which is required to be smooth across the boundary ( $\frac{\partial E}{\partial n} = 0$ ). In contrast, the tangential  $H$  field is constrained in a different manner ( $\frac{1}{\epsilon} \frac{\partial H}{\partial n} = 0$ ). Consequently, the  $H$  field could be more localized within the high dielectric region than the  $E$  field. In addition, the respective eigenmodes display one higher order of oscillations than those in TE polarization; one pair of oscillations is associated with the lower edge [Fig. 4(a)] and two pairs are with the upper edge [Fig. 4(b)].

The drastic change of field patterns between Figs. 3(a) and 3(b) [or Figs. 4(a) and 4(b)] accompanies a notable difference of resonance frequency between the lower and the upper edges, which makes up the band gap width. This distinction is also identified in terms of multipole-like fields: the magnetic dipole [Fig. 3(a)] and quadrupole [Fig. 3(b)] for TE modes, and the electric quadrupole [Fig. 4(a)] and octupole [Fig. 4(b)] for TM modes. This will be more realized when the band gap features are correlated to Mie resonances and waveguide modes, as discussed in the next two subsections.

### 3.2. Connection with Mie resonances

The higher-lying band gap features reported in Figs. 2–4 are closely related to Mie resonance in two aspects. First, the upper and lower band edges are approximately *bounded* by the Mie resonance frequencies of successive two orders. The TE band edges occur near the first and second Mie resonances with the same polarization, while the TM band edges locate near the second and third Mie resonances. Second, the respective eigenmodes exhibit similar *internal* field patterns with the Mie resonance modes. This means that resonances on single scatterers dominate the dispersion characteristics (around the band edges) in the underlying problem. This

feature also responds to the dispersionless behavior (insensitive to the change of Bloch's wave vector) for the corresponding frequency branches.

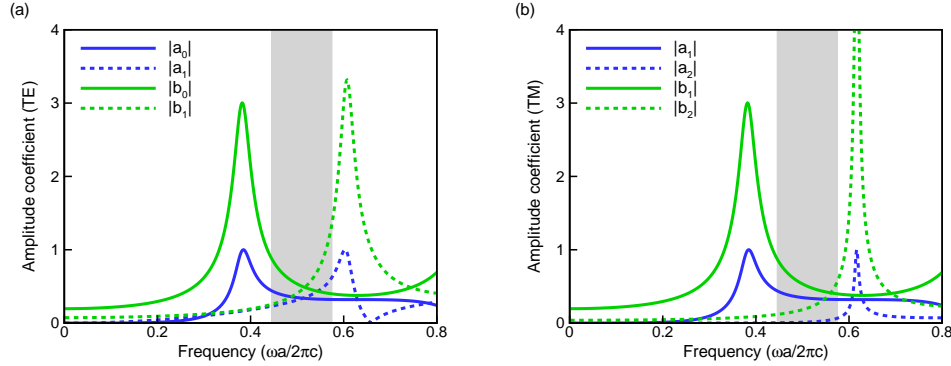


Fig. 5. Amplitude coefficients of the scattered and internal fields for a dielectric circular cylinder of radius  $r = 0.19a$  and dielectric constant  $\epsilon_d = 26$ . (a) TE polarization, (b) TM polarization. Shaded areas correspond to the common band gap region for the photonic crystal in Fig. 2. Vertical solid and dashed lines indicate the waveguide mode frequencies related to Mie resonances.

Mie resonance is the scattering excitation of a single scatterer [27], which occurs when the wavelength matches the size of scatterer. At resonance, the scattered and internal fields may be strongly enhanced. For a dielectric circular cylinder of radius  $r$  and dielectric constant  $\epsilon_d$ , the scattered and internal fields subject to an incident plane wave are given as [28]

$$H^{\text{scat}} = \sum_{n=-\infty}^{\infty} a_n H_n(k\rho) e^{-in\phi}, \quad a_n = i^n \frac{J_n(x)J'_n(x_1) - \sqrt{\epsilon_d}J'_n(x)J_n(x_1)}{\sqrt{\epsilon_d}H'_n(x)J_n(x_1) - H_n(x)J'_n(x_1)}, \quad (5)$$

$$H^{\text{int}} = \sum_{n=-\infty}^{\infty} b_n J_n(\sqrt{\epsilon_d}k\rho) e^{-in\phi}, \quad b_n = i^n \frac{2i/\pi x}{\sqrt{\epsilon_d}H'_n(x)J_n(x_1) - H_n(x)J'_n(x_1)}, \quad (6)$$

for TE polarization, where  $\rho$  and  $\phi$  are cylindrical coordinates with the origin at the cylinder center,  $x \equiv kr = \omega r/c$ ,  $x_1 \equiv \sqrt{\epsilon_d}x$ ,  $J_n(x)$  and  $H_n(x)$  are the  $n$ th order Bessel function and Hankel function of the first kind, respectively, the prime denotes derivative with respect to the argument, and the dielectric constant of surrounding medium is assumed to be unity. Mie resonance corresponds to divergence of the amplitude coefficients for the scattered and internal fields; that is, the vanishing denominator of  $a_n$  or  $b_n$  [29]. Let  $r = 0.19a$  and  $\epsilon_d = 26$  be the same as the photonic structure in Fig. 2. The first two orders of  $a_n$  and  $b_n$  for TE polarization are plotted in Fig. 5(a), where the Mie resonances (located at the peak positions) occur at  $\omega = 0.382(2\pi c/a)$  and  $\omega = 0.607(2\pi c/a)$ . For comparison, the common gap region for the photonic crystal in Fig. 2 is overlaid in the same plot (shaded area), showing that the common gap region is approximately bounded by the two Mie resonance frequencies. The corresponding internal field is given by  $H_{nm}^{\text{int}} = J_n(\sqrt{\epsilon_d}x_{nm}\rho/r)\cos(n\phi)$ , where  $x_{nm}$  is the  $m$ th zero of the denominator of  $a_n$  or  $b_n$ . The field patterns for  $H_{01}^{\text{int}}$  and  $H_{11}^{\text{int}}$  are shown in Figs. 6(a) and 6(b), respectively. A notable similarity is observed with the respective eigenmodes (in the dielectric region) for the photonic crystal [cf. Figs. 3(a) and 3(b)]. This feature further confirms the correlation of Mie resonances to the higher-lying band gaps in the present problem.

For TM polarization, similar expressions are given for the scattered and internal fields as [28]

$$E^{\text{scat}} = \sum_{n=-\infty}^{\infty} a_n H_n(k\rho) e^{-in\phi}, \quad a_n = i^n \frac{\sqrt{\epsilon_d}J_n(x)J'_n(x_1) - J'_n(x)J_n(x_1)}{H'_n(x)J_n(x_1) - \sqrt{\epsilon_d}H_n(x)J'_n(x_1)}, \quad (7)$$

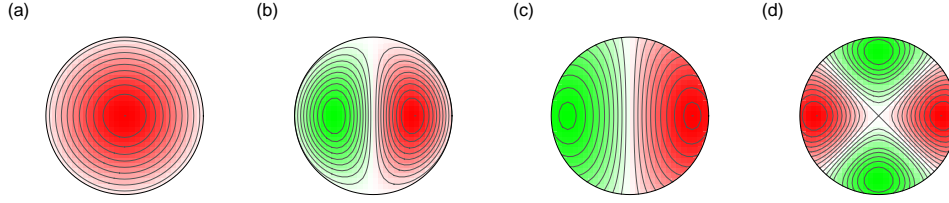


Fig. 6. Internal field patterns of Mie resonances for a dielectric circular cylinder of radius  $r = 0.19a$  and dielectric constant  $\epsilon_d = 26$ . (a)  $H_{01}^{\text{int}}$  field with  $\omega = 0.382(2\pi c/a)$ , (b)  $H_{11}^{\text{int}}$  field with  $\omega = 0.607(2\pi c/a)$ , (c)  $E_{11}^{\text{int}}$  field with  $\omega = 0.382(2\pi c/a)$ , (d)  $E_{21}^{\text{int}}$  field with  $\omega = 0.617(2\pi c/a)$ .

$$E^{\text{int}} = \sum_{n=-\infty}^{\infty} b_n J_n(\sqrt{\epsilon_d} k \rho) e^{-in\phi}, \quad b_n = i^n \frac{2i/\pi x}{H_n'(x)J_n(x_1) - \sqrt{\epsilon_d} H_n(x)J_n'(x_1)}, \quad (8)$$

where the amplitude coefficients are plotted in Fig. 5(b) for the same  $r$  and  $\epsilon_d$ . The peaks of the second and third orders of  $a_n$  and  $b_n$  occur at  $\omega = 0.382(2\pi c/a)$  and  $0.617(2\pi c/a)$ , respectively. As in the case of TE polarization, the common gap region is approximately bounded by the two Mie resonance frequencies. Note that the peak of  $a_1$  ( $b_1$ ) in TM modes coincides with that of  $a_0$  ( $b_0$ ) in TE modes, which can be realized by the relations:  $J_0' = -J_1$  and  $H_0' = -H_1$ . In addition, the connection with the zeroth order coefficients  $a_0$  and  $b_0$  is not obvious. This is in accordance with the observation that the band gap locates at relatively higher bands for TM polarization (cf. Fig. 2). The internal field is given by  $E_{nm}^{\text{int}} = J_n(\sqrt{\epsilon_d} x_{nm} \rho / r) \cos(n\phi)$ , as shown in Figs. 6(c) and 6(d) for  $E_{11}^{\text{int}}$  and  $E_{21}^{\text{int}}$ , respectively. As expected, the Mie resonance modes display similar field patterns with the respective eigenmodes (in the dielectric region) for the photonic crystal [cf. Figs. 4(a) and 4(b)].

### 3.3. Related waveguide modes

It is noticed that the Mie resonances stated above can be closely related to waveguide modes, but with mutually *exchanged* polarizations. For sufficiently large  $\epsilon_d$ , Mie resonance condition for TE polarization is approximated to  $J_n(\sqrt{\epsilon_d} x) \approx 0$  [the vanishing denominator of Eq. (5) or (6)], which is the boundary condition for TM waveguides [30]. The frequency of  $\text{TM}_{nm}$  waveguide mode is given as  $\omega_{nm}^{\text{TE}} = x_{nm} c / r \sqrt{\epsilon_d}$ , where  $x_{nm}$  is the  $m$ th zero of  $J_n(x)$ . For the same geometry and material ( $r = 0.19a$  and  $\epsilon_d = 26$ ), the lowest two modes occur at  $\omega_{01}^{\text{TM}} = 0.395(2\pi c/a)$  and  $\omega_{11}^{\text{TM}} = 0.629(2\pi c/a)$  ( $x_{01} \approx 2.405$  and  $x_{11} \approx 3.832$ ), which are close to Mie resonance frequencies at  $0.382(2\pi c/a)$  and  $0.607(2\pi c/a)$ , respectively [cf. Figs. 6(a) and 6(b)].

Likewise, Mie resonance condition for TM polarization is approximated (but not as good as the TE case) to  $J_n'(\sqrt{\epsilon_d} x) \approx 0$  [the vanishing denominator of Eq. (7) or (8)] for large  $\epsilon_d$ . This is the boundary condition for TE waveguides [30], and the frequency of  $\text{TE}_{nm}$  waveguide mode is given as  $\omega_{nm}^{\text{TM}} = x'_{nm} c / r \sqrt{\epsilon_d}$ , where  $x'_{nm}$  is the  $m$ th zero of  $J_n'(x)$ . Accordingly, the second and third modes occur at  $\omega_{11}^{\text{TE}} = 0.302(2\pi c/a)$  and  $\omega_{21}^{\text{TE}} = 0.502(2\pi c/a)$  ( $x'_{11} \approx 1.841$  and  $x'_{21} \approx 3.054$ ), respectively. Note that both  $\omega_{11}^{\text{TE}}$  and  $\omega_{21}^{\text{TE}}$  are not so close to Mie resonances at  $0.382(2\pi c/a)$  and  $0.617(2\pi c/a)$ , respectively [cf. Figs. 6(c) and 6(d)]. This is due to the *weaker* localization of fields (inside the dielectric) in TM polarization (compare Figs. 3 and 4), so that TM waveguide modes are not indeed very accurate approximations to Mie resonances. Nonetheless, they serve as a convenient way for roughly estimating the Mie resonances and describing the band gap features of the underlying problem.

#### 4. Concluding remarks

In conclusion, the higher-lying band gaps for two-dimensional photonic crystals are investigated, with emphasis on the resonance features and related mechanism. An optimal common band gap width  $[0.129(2\pi c/a)]$  with the gap to mid-gap ratio (25.3%) was attained on a hexagonal lattice of circular cylinders ( $r/a = 0.19$ ) with large dielectric contrast ( $\epsilon_d = 26$ ). The high permittivity can be achieved by using the ceramic as the dielectric material, whose dielectric constant may range from twenties to thirties [31]. The feature of higher band gap holds for lower index contrast as well, but is not optimal; for instance, the band gap ratio for a silicon-based structure with the same geometry is 10.4%. In the present problem, an obvious distinct feature from the fundamental band gap is the opening of gap region between two consecutive dielectric-like bands, where the fill factor for measuring the energy concentration does not exhibit a marked difference. The apparent change of eigenmode patterns inside the cylinders, which occurs simultaneously for TM and TE modes, is responsible for a large higher-lying common band gap. At the optimal condition, the band edges for both polarizations are nearly located at the same positions, around which the frequency branches tend to be dispersionless (flattened) due to the strong localization of fields inside the dielectric regions. It follows that the eigenmodes at the two band edges are analogous to Mie resonances and related waveguide modes. The field patterns (inside the cylinder) exhibit a sudden change from dipole to quadrupole oscillations (TE polarization), or from quadrupole to octupole ones (TM polarization), between two consecutive eigenmodes for the photonic crystal, which occur as well between two successive orders of Mie resonances.

#### Acknowledgments

This work was supported in part by National Science Council of the Republic of China under Contract No. NSC 96-2221-E-002-190-MY3 and NSC 97-2120-M-002-013.